

Periodically driven perturbed CFTs: the sine-Gordon model

Zoltán Bajnok¹, Robin Oberfrank^{1,2}

April 1, 2025

¹*Wigner Research Centre for Physics
Konkoly-Thege Miklós u. 29-33, 1121 Budapest, Hungary*
²*Roland Eötvös University
Pázmány s. 1/A, 1117 Budapest, Hungary*

Abstract

We analyze a version of the sine-Gordon model in which the strength of the cosine potential has a periodic dependence on time. This model can be considered as the continuum limit of the many body generalization of the Kapitza pendulum. Based on the perturbed CFT point of view, we develop a truncated conformal space approach (TCSA) to investigate the Floquet quasienergy spectrum. We focus on the effective behaviour for large driving frequencies, which we also derive exactly. Depending on the driving protocol, we can recover the original sine-Gordon model or its two-frequency version. The rich structure of the two-frequency model implies that the time-periodic drive can break integrability, can lead to new states in the spectrum or can result in a phase transition. Our method is applicable for any periodically driven perturbed conformal field theories.

Contents

1	Introduction	2
2	Classical considerations	3
2.1	Kapitza pendulum	4
2.2	Many body generalization: the sine-Gordon model	5
3	Quantum models	7
3.1	Floquet theory and the Kapitza pendulum	7
3.2	The periodically driven sine-Gordon model	8
3.2.1	Sine-Gordon model as a perturbed CFT	9
3.2.2	Periodic drive	10
4	Numerical investigations and results	12
4.1	Floquet quasienergy spectrum	12
4.2	Effective Hamiltonian	14
5	Periodically driven perturbed CFTs	17
6	Conclusion	18
A	Large frequency expansion and a numerical approach	19
B	TCSA and the driven sine-Gordon model	21
C	Calculation of the effective Hamiltonian for generic pertrubed CFTs	24

1 Introduction

The equilibrium behaviour of isolated statistical physical systems are successfully described and understood [1]. Recently, the focus of the investigations has been shifted to the far from equilibrium domain, partly due to the advancement of cold atom experiments. By introducing various protocols, the system can be driven away from the equilibrium and the main problem is to understand its long time behaviour. Typically, we let the originally closed quantum system to interact with its environment. This can be a sudden change in the boundary conditions or in the parameters of the theory and often we close the system again after this quench and we investigate the relaxation towards equilibrium [2].

Alternatively, we can subject the system to a periodic driving force and investigate its time evolution. In many cases, the driven interacting system becomes ergodic and visits the whole phase space in the classical case or heats to infinite temperature in the quantum case. However, there is a large class of models when this does not happen and the system remains stable. The periodic drive can lead to universal high frequency behaviour, which leads to dynamical stabilization and can be used in Floquet engineering, a topic very intensively investigated recently [3].

A particularly interesting case is when the originally unstable fix points become stable. A prototypical example is the Kapitza pendulum [4], a rigid pendulum in which the pivot point is

moved harmonically in the vertical direction. For large enough driving frequencies the upper unstable equilibrium point can be dynamically stabilized by this periodic drive. The field theoretical limit of the many-body generalization of the Kapitza pendulum is the periodically driven sine-Gordon model [5], which was analyzed by various approximate methods and the dynamical stability was indicated. The authors also suggested an experimental realization in an ultracold atom experiment, in which the atoms are trapped into two parallel one dimensional lines by a transversal confinement potential generated through standing laser waves. By modulating the amplitude of the transverse field a time-dependent tunneling coupling between the two parallel tubes can be induced realizing the drive needed for the sine-Gordon model.

In the present paper, we would like to go beyond the methods and the focus of [5] and would like to analyze the quasienergy spectrum of the driven sine-Gordon theory. This will be done by exploiting that the sine-Gordon theory can be considered as a perturbed conformal field theory (CFT). This allows us to use analytical and very successful numerical methods to investigate the system. The truncated conformal space approach (TCSA) [6] proved to be a useful tool to analyze various observables in perturbed conformal field theories and our aim is to combine it with the usual numerical method of the periodically driven systems to calculate the spectrum of the Floquet Hamiltonian. We are going to identify a protocol when the infinite frequency effective theory becomes the two-frequency sine-Gordon model [7, 8] allowing us to see the dynamical stabilization of unstable fix points and reach very nontrivial limiting theories. Our approach paves the way to investigate periodically driven perturbed conformal field theories with the same methods. In the formulation of our approach we take a pedagogical path and introduce all concepts in simplified circumstances.

The paper is organized as follows: we start in section 2 by recalling the dynamical stabilization and separation of time scales in the example of the Kapitza pendulum, which is basically the zero mode of the driven sine-Gordon theory. We also emphasize the possibility of introducing different driving protocols, depending on how we scale the amplitude of the drive with the frequency. By coupling many Kapitza pendula and taking their continuum limit, we arrive at the driven sine-Gordon theory, whose stability we analyze in the small amplitude limit, where we can see that stability can be ensured only in a finite volume or with a momentum cutoff. We then turn to the quantum theory in section 3. Floquet theory, the quantum approach to periodically driven systems is introduced on the example of the quantum Kapitza pendulum, together with the standard numerical method based on Fourier transformation to calculate the quasienergy spectrum and an analytical method to derive the large frequency expansion [9]. Having introduced the sine-Gordon theory as a perturbed CFT together with its TCSA method [10], we specify the previous findings to deal with the periodical drive. We also perform analytical calculations and reveal the importance of scaling the amplitude of the drive. The numerical investigations and their interpretations are summarized in section 4. The analytical calculation for the large frequency effective behaviour is extended for generic perturbed conformal field theories in Section 5. Finally, we conclude in section 6. Technical details are relegated to Appendices.

2 Classical considerations

In this section, we review the classical theory and introduce the separation of scales as well as the large frequency expansion.

2.1 Kapitza pendulum

The Kapitza pendulum is a rigid pendulum in which the pivot point is moved harmonically in the vertical direction [4]. The Hamiltonian has the form

$$H = \frac{p_\phi^2}{2} + c(t)(1 - \cos \phi) \quad ; \quad c(t) = c_0 + c_1 \cos \omega t \quad (1)$$

where ϕ is the 2π periodic angle variable and the driving is controlled by c_1 . Without the drive, the system has two equilibrium points: $\phi = 0$ is stable, while $\phi = \pi$ is unstable. For large enough driving frequencies, however, the unstable fix point becomes stable. This counterintuitive phenomenon can be understood in the effective description, in which the motion is separated into an average slow and a periodic fast motion

$$\phi(t) = \Phi(t) + \xi(t) \quad ; \quad \xi(t + T) = \xi(t) \quad (2)$$

where $T = \frac{2\pi}{\omega}$ and $\int_{t-T/2}^{t+T/2} \phi(t) dt = \Phi(t)$. There is a systematic expansion in ω^{-2} , see [9] for details, which at the leading order gives

$$\xi = \frac{c_1}{\omega^2} \cos \omega t \sin \Phi \quad ; \quad \ddot{\Phi} = -\frac{d}{d\Phi} \left(c_0(1 - \cos \Phi) + \frac{c_1^2}{4\omega^2} \sin^2 \Phi \right) \equiv -\frac{dU_{\text{eff}}(\Phi)}{d\Phi} \quad (3)$$

Thus, there is a small-amplitude, large-frequency motion with vanishing time average and a slow motion in an effective potential. The new term in the effective potential makes the upper equilibrium point stable as demonstrated on Figure 1.

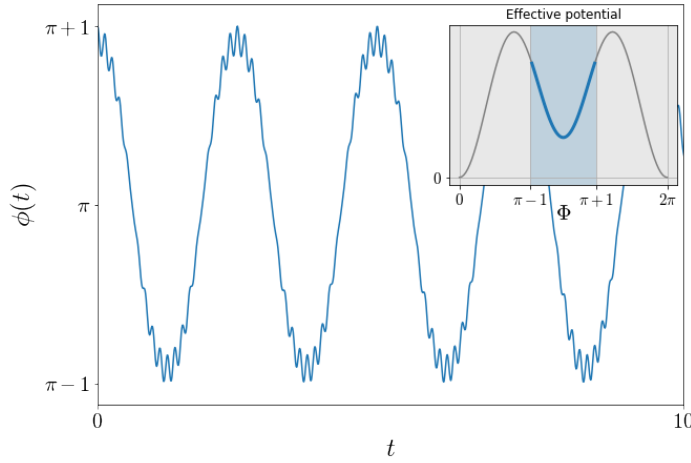


Figure 1: Periodic motion around the upper equilibrium point obtained by solving the equation of motions with the periodic drive, and the corresponding effective potential.

Depending on how the amplitude of the drive scales with ω , we can see different behaviours:

- For ω -independent $c_1 = \lambda$, the drive averages out in the large ω limit, and the effective motion is the same as the one without the drive. It can be understood physically as the drive is oscillating so fast so that the system with a finite inertia cannot follow it.

- This is drastically changed if the drive scales with ω : $c_1 = \lambda\omega$. In this case, the fast oscillation vanishes in the large ω limit, and the motion is basically as it would happen in the effective, ω -independent potential $U_{\text{eff}}(\Phi) = c_0(1 - \cos \Phi) + \frac{\lambda^2}{4} \sin^2 \Phi$. For $\frac{\lambda^2}{2} > c_0$, both equilibria are stable.
- In the case of the Kapitza pendulum the drive is proportional to ω^2 : $c_1 = \lambda\omega^2$. The small fluctuations are ω -independent, but the effective potential does not have a finite $\omega \rightarrow \infty$ limit. In this case, ω is kept finite and the system has a rich stability diagram.

The stability of the two equilibria can be understood in the small-angle limit, $\phi \sim \epsilon, \pi + \epsilon$, i.e. $\sin \phi \sim \pm \epsilon$ when the equation of motion can be mapped to the Mathieu equation

$$y''(x) + (a - 2q \cos 2x)y(x) = 0 \quad ; \quad (a, q, x) \leftrightarrow \left(\pm \frac{4c_0}{\omega^2}, \frac{2c_1}{\omega^2}, \frac{\omega t}{2} \right) \quad (4)$$

with a well-known stability diagram (see Figure 2). The upper equilibrium appears for $a < 0$, while the lower one for $a > 0$. Clearly, for the Kapitza pendulum $c_1 = \lambda\omega^2$, the upper fix point becomes stable above a λ -dependent critical frequency.

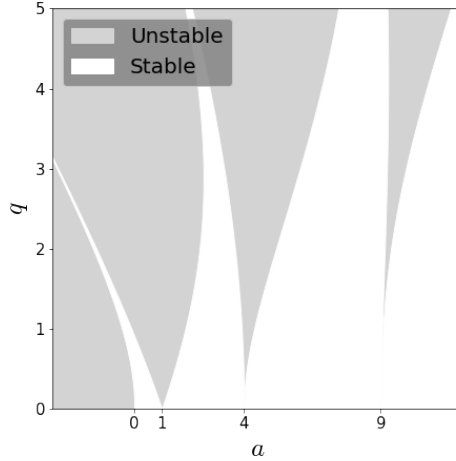


Figure 2: Stability diagram of the Mathieu equation. Stable regions correspond to bounded oscillations, while unstable ones mean exponentially growing solutions.

In the following sections, we focus on the case when the effective potential has a finite non-trivial $\omega \rightarrow \infty$ limit, and investigate the continuum limit of the many body generalization of this model.

2.2 Many body generalization: the sine-Gordon model

If we take many pendula on a line, couple them with torsion springs and take the continuum limit we obtain the sine-Gordon field theory with infinite degrees of freedom, see eg. [11]. Doing the same with many Kapitza pendula leads to the driven sine-Gordon model [5]:

$$\partial_t^2 \phi(x, t) - \partial_x^2 \phi(x, t) + (c_0 + c_1 \cos \omega t) \sin \phi(x, t) = 0 \quad (5)$$

The stability of the system around the $\phi(x, t) = 0, \pi$ configurations can be analyzed by approximating $\sin \phi \sim \pm \phi$ and decoupling the modes in Fourier space. The resulting equation of motion for the k th mode $\phi(x, t) \propto \phi_k(t)e^{ikx}$ can again be mapped to the Mathieu equation

$$\partial_t^2 \phi_k \pm (c_0 \pm k^2 + c_1 \cos \omega t) \phi_k = 0 \quad ; \quad (a, q) \leftrightarrow \left(4 \frac{\pm c_0 + k^2}{\omega^2}, \frac{2c_1}{\omega^2} \right) \quad (6)$$

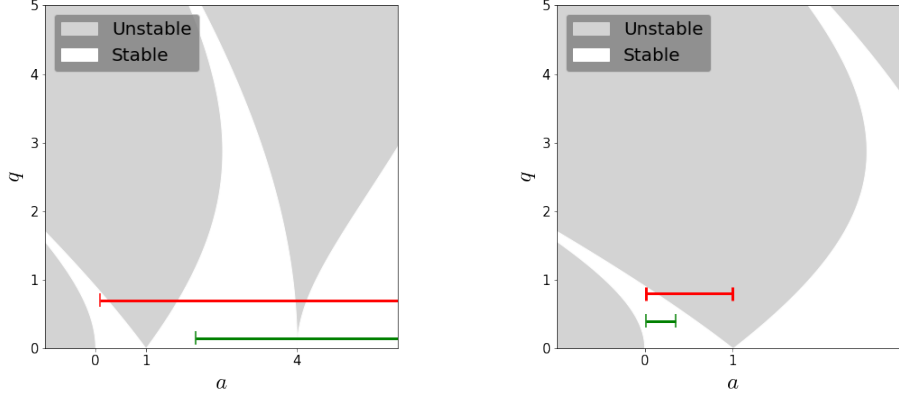


Figure 3: Small fluctuations of the periodically driven sine-Gordon equation are mapped to the stability diagram of the Mathieu equation for various parameters. Red lines correspond to evolving field configurations with resonant modes, green ones have stable evolution. Left figure shows solutions localized to the lower fix point, where the momentum cutoff is not necessary, while on the right, we see solutions localized to the upper fix point, where the cutoff has to be used to avoid the resonant modes.

Since in the field theory, we have a continuum of modes $k \in \mathbb{R}$, whatever c_0 and c_1 we choose we always cross the instability regions, see Figure 3. The reason is that in our small-field decoupled harmonic oscillator limit, we always have a mode, which resonates with the driving frequency leading to parametric resonance. To avoid this, we could put the system in a finite volume L , and then the possible k values will be quantized: $k_n = \frac{n2\pi}{L}$, and we might avoid the discrete points that lie within the unstable regions. In the large volume limit, however, we should always face some instabilities. We could also introduce a momentum cutoff k_{\max} , and choose a large enough driving frequency, such that the corresponding allowed (a, q) values always lie in the stability region. This is actually the typical case as in many applications, the sine-Gordon model is an approximation, and the real physical system has a built in ultra-violet cutoff.

With this trick, we can even make the upper fix point, $\phi = \pi$ stable. This configuration then can serve as another vacuum and excitation such as the breather can live over them. We demonstrate this by explicitly solving the equation of motion (see Figure 2.2). In our approach, we used the Chebyshev spectral method to calculate the time evolution.

It is a conceptually interesting question whether the stability survives in the quantum theory or not. Clearly at the quantum level, the excitations are quantized and they cannot be arbitrarily small, thus the small ϕ expansion is not adequate. Indeed, in the sine-Gordon theory, the small fluctuations correspond to breather excitations, which are the elementary

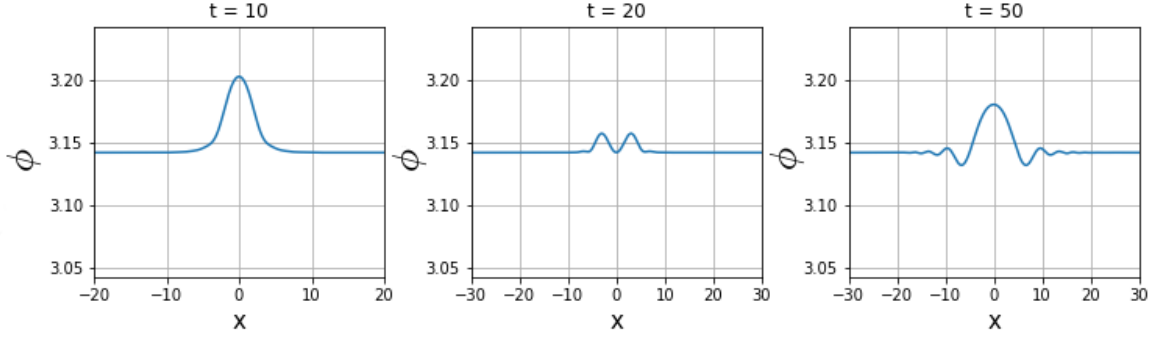


Figure 4: Time evolution of a breather type configuration at the upper fix point with parameters: $c_1 = \lambda\omega^2$, $\lambda = 0.1$, $\omega = 100$, $c_0 = 1$. This configuration does not decay, but slowly radiates due to non-integrable effects [12].

quanta of the field with finite masses. Depending on the coupling, the masses vary and the breathers can even leave the spectrum, such that only solitons remain. This makes the quantum theory stable as we will see. In the quantum analysis, we will introduce both a finite volume and a momentum cutoff, and will focus on the large-frequency limit, varying both the volume and the cutoff, too.

3 Quantum models

In this section, we introduce the Floquet theory of periodically driven systems together with their large frequency expansion and develop a numerical method to investigate the spectrum of the quasienergies. We start with the quantum version of the Kapitza pendulum. We then present the sine-Gordon theory, where we exploit its perturbed CFT formulation.

3.1 Floquet theory and the Kapitza pendulum

In the quantum theory, we investigate the time evolution of the system with an explicit harmonic-type time-dependent Hamiltonian

$$i\frac{\partial\Psi}{\partial t} = H\Psi \quad ; \quad H = H_0 + V_0 + \cos\omega t V_1 \quad (7)$$

i.e. V_0, V_1 will not depend explicitly on time. In the case of the Kapitza pendulum, they take the form

$$H_0 = \frac{p_\phi^2}{2} \quad ; \quad V_0 = c_0(1 - \cos\phi) \quad ; \quad V_1 = c_1 \cos\phi \quad (8)$$

The separation of scales has a quantum analogue [9], which is phrased in Floquet theorem: for periodic Hamiltonians $H(t) = H(t + T)$ the solution of the Schrödinger equation can be expanded in a basis $\psi_{\mathcal{E}}$ evolving as

$$\psi_{\mathcal{E}}(\phi, t) = e^{-i\mathcal{E}t} u_{\mathcal{E}}(\phi, t) \quad (9)$$

where $u_{\mathcal{E}}(\phi, t + T) = u_{\mathcal{E}}(\phi, t)$. The quasienergy \mathcal{E} governs the slow motion in an effective potential, while the periodic $u_{\mathcal{E}}$ is the analogue of the fast modulation. In order to find the effective Hamiltonian, which is unitary equivalent to the operator that generates the evolution with one period of time, one can make a periodic gauge transformation [9] of the form $u_{\mathcal{E}}(\phi, t) = e^{-iF(t)}v_{\mathcal{E}}(\phi)$ leading to

$$H_{\text{eff}} = e^{iF} H e^{-iF} - i(\partial_t e^{iF}) e^{-iF} \quad (10)$$

where F and H_{eff} can be calculated simultaneously order by order in ω^{-1} , see appendix A, and at the leading and non-vanishing subleading order we get

$$H_{\text{eff}} = H_0 + V_0 + \frac{1}{4\omega^2} [[V_1, H_0 + V_0], V_1] + O(\omega^{-4}) \quad (11)$$

This calculation is quite general, which relies only on the specific time dependence of the perturbation $\cos \omega t V_1$, but not on the specific form of V_0, V_1 and will be valid also in the quantum field theory. In the generic case of a single particle, the effective Hamiltonian is

$$H_{\text{eff}} = \frac{p_{\phi}^2}{2} + V_0 + \frac{1}{4\omega^2} (\partial_{\phi} V_1)^2 + O(\omega^{-4}) \quad (12)$$

Clearly, for the Kapitza pendulum, this yields the same effective potential U_{eff} as in (3), which is the quantum analogue of the classical dynamics. In the more general case when V_0 and V_1 are equivalent up to a linear term in the coordinate, this maps all unstable fix points of V_0 to stable ones.

In order to test the above large-frequency approximation, we can determine numerically the Floquet basis, which satisfies the modified Schrödinger equation:

$$H_F u_{\mathcal{E}}(\phi, t) = \mathcal{E} u_{\mathcal{E}}(\phi, t) \quad ; \quad H_F = H - i\partial_t \quad (13)$$

Since $u_{\mathcal{E}}(\phi, t)$ is periodic in time, we simply expand it in Fourier components: $u_{\mathcal{E}}(\phi, t) = \sum_m u_{\mathcal{E},m}(\phi) e^{im\omega t}$ such that the eigenvalue problem takes the form

$$(m\omega + H_0 + V_0) u_{\mathcal{E},m} + \frac{1}{2} V_1 (u_{\mathcal{E},m-1} + u_{\mathcal{E},m+1}) = \mathcal{E} u_{\mathcal{E},m} \quad (14)$$

We can further expand $u_{\mathcal{E},m}(\phi)$ in the eigenbasis of H_0 , and formulate an equation in the double discrete infinite basis, see Appendix A for details. The numerical solution showed (see Figure 5) that for large ω , the effective description is recovered correctly, and from the eigenvectors, we can recognize states localized around the upper equilibrium point.

3.2 The periodically driven sine-Gordon model

The quantum version of the periodically driven sine-Gordon model shares the same structure of the Hamiltonian as the Kapitza pendulum (7) but we are in a quantum field theory where the system is confined into a finite volume L as

$$H_0 = \frac{1}{8\pi} \int_0^L dx : (\partial_t \phi)^2 - (\partial_x \phi)^2 : \quad ; \quad V_i = c_i \int_0^L dx : \cos \beta \phi : \quad (15)$$

and the normal ordering is defined wrt. the free compactified massless boson of radius $r = \beta^{-1}$ [10, 11].

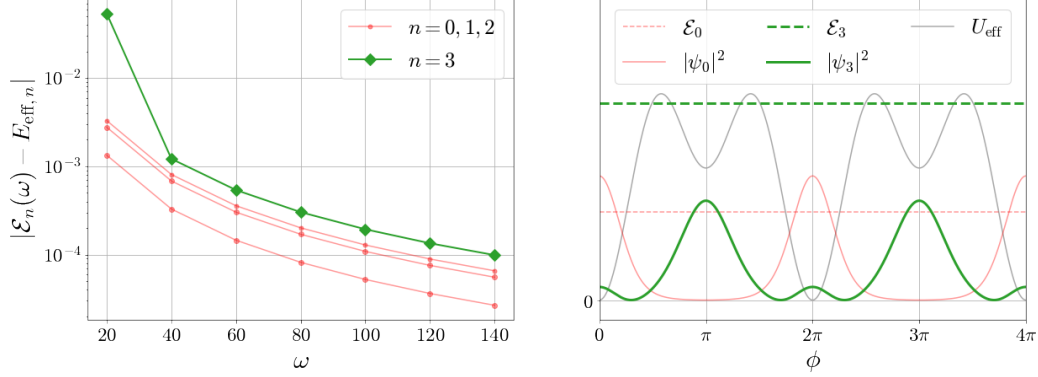


Figure 5: Comparison of the large ω Floquet quasienergy spectrum with the spectrum of the effective Hamiltonian is shown on the left, while wave functions localized around the two stable fix points are demonstrated on the right. Parameters: $c_1 = \lambda, c_0 = 0.5, \lambda = 2$.

3.2.1 Sine-Gordon model as a perturbed CFT

Since we work with the free compactified boson, ϕ is regarded as an angle variable with the identification $\phi + 2\pi r \equiv \phi$. This implies that boundary conditions can be labeled by the integer winding number m as $\phi(x + L, t) = \phi(x, t) + 2\pi r m$, which distinguishes topological sectors closed for time evolutions. The zero mode $\phi_0(t) = L^{-1} \int_0^L \phi(x, t) dx$, behaves as a single pendulum. In the free theory, its conjugate momentum π_0 , satisfying $[\pi_0, \phi_0] = -i$, has the spectrum $\pi_0 |n\rangle = \frac{n}{r} |n\rangle$ with integer n . The other modes ϕ_n can be expanded in terms of creation and annihilation operators, see Appendix B for details. Since the free massless boson is a conformal field theory, it is customary to work on the plane defined by the conformal mapping $z = e^{i\frac{2\pi}{L}(x+t)}$, $\bar{z} = e^{-i\frac{2\pi}{L}(x-t)}$. Conformal symmetry implies that the field separates into independent left and right moving parts and the full Hilbert space is built over the states with given winding and momentum numbers by acting with the left and independent right moving creation operators:

$$\mathcal{H} = \sum_{n, m \in \mathbb{Z}} \mathcal{V}_{n, m} \otimes \bar{\mathcal{V}}_{n, m} \quad ; \quad \mathcal{V}_{n, m} = \{a_{-n_1} \dots a_{-n_k} |n, m\rangle\} \quad (16)$$

where $[a_n, a_m] = n\delta_{n+m, 0}$ and similarly for $\bar{\mathcal{V}}_{n, m}$ with the appropriate changes. The Hamiltonian and the total momentum are

$$H_0 = \frac{2\pi}{L} \left(L_0 + \bar{L}_0 - \frac{1}{12} + \pi_0^2 + \frac{m^2 r^2}{4} \right) \quad ; \quad P_0 = \frac{2\pi}{L} (L_0 - \bar{L}_0 + \pi_0 m) \quad (17)$$

where $L_0 = \sum_{k>0} a_{-k} a_k$ and $\bar{L}_0 = \sum_{k>0} \bar{a}_{-k} \bar{a}_k$. The perturbing operator can also be mapped onto the plane. As $:e^{i\beta\phi}:$ is a primary field of weights $(h, \bar{h}) = (\frac{\beta^2}{2}, \frac{\beta^2}{2})$ the perturbation takes the form

$$V_i = c_i \left(\frac{L}{2\pi} \right)^{1-\beta^2} \hat{V}_1 \quad ; \quad \hat{V}_1 = \int_0^{2\pi} d\theta \frac{1}{2} \left(V^\beta(e^{i\theta}, e^{-i\theta}) + V^{-\beta}(e^{i\theta}, e^{-i\theta}) \right) \quad (18)$$

where the normal ordered vertex operator on the plane was introduced $V^\beta(z, \bar{z}) =: e^{i\beta\phi(z, \bar{z})} :.$ Without the drive, $c_1 = 0$, normal ordering is enough to regularize the theory for $\beta^2 < 1$. In this region, the theory contains breather and soliton excitations. The only dimensionful perturbing parameter c_0 sets the scale and it is related to the soliton mass M as [13]:

$$c_0 = \kappa(h)M^{2-2h} \quad ; \quad \kappa(h) = \frac{2\Gamma(h)}{\pi\Gamma(1-h)} \left(\frac{\sqrt{\pi}\Gamma(\frac{1}{2(1-h)})}{2\Gamma(\frac{h}{2(1-h)})} \right)^{2-2h} \quad (19)$$

The truncated conformal space approach can be used to calculate the spectrum [6]. It amounts to truncate the Hilbert space at a given energy, E_{cut} , and to calculate the finite matrix representations of the Hamiltonian $H_0 + V_0$ and then diagonalize them [10]. A typical spectrum can be seen on Figure 6.

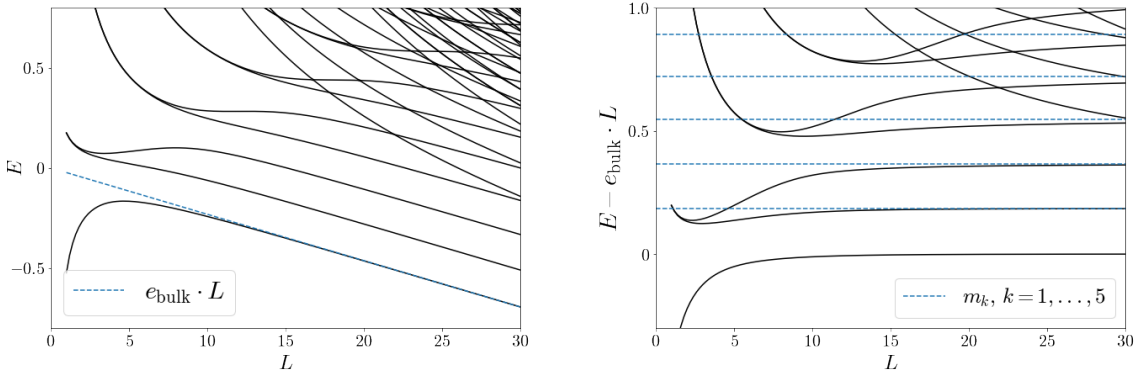


Figure 6: Typical TCSA spectrum of the sine-Gordon theory. Here and from now on we always choose $r = 3$, $M = 1$. On the left is the raw spectrum, while on the right we subtract the exactly known bulk groundstate energy. Breather masses are indicated by dashed lines.

Since this is an integrable quantum field theory, the finite size spectrum is completely known [14, 15]. The bulk energy constant is $e_{\text{bulk}} = -\frac{M^2}{4} \tan \frac{\pi p}{2}$, where $h = \frac{p}{1+p} = \frac{\beta^2}{2}$, while the mass of the k^{th} breather is $m_k = 2M \sin \frac{\pi p k}{2}$.

For $1 < \beta^2$ the perturbing operator is not well-defined [16]. The spectrum does not stabilize in the $E_{\text{cut}} \rightarrow \infty$ limit and one has to subtract an E_{cut} -dependent diverging constant. This can be avoided by analyzing energy differences only. For higher β s, even energy differences are not enough to consider and one has to introduce an E_{cut} -dependent operator counter term [16, 17]. Above $\beta^2 = 2$, the TCSA method cannot be used, as we cross the Kosterlitz-Thouless phase transition and the perturbation becomes irrelevant.

3.2.2 Periodic drive

Let us now analyze the effect of the periodic drive. If the drive is turned on, we are interested in the Floquet quasienergy spectrum. The large ω expansion follows the calculation of the Kapitza pendulum and leads to the effective Hamiltonian (11), which in dimensionless

quantities in our case reads as

$$H_{\text{eff}} = \frac{2\pi}{L} \left[\hat{H}_0 + \frac{c_0}{2} \left(\frac{L}{2\pi} \right)^{2-\beta^2} \hat{V}_1 + \left(\frac{L}{2\pi} \right)^{2-2\beta^2} \frac{c_1^2}{4\omega^2} [[\hat{V}_1, \hat{H}_0], \hat{V}_1] \right] + O(\omega^{-4}) \quad (20)$$

We calculate the commutator $[[\hat{V}_1, \hat{H}_0], \hat{V}_1]$ in Appendix B analytically. As the expression contains products of operators at the same points, the commutator is not well-defined and needs to be regularized. By introducing a mode number cutoff, we keep only the oscillators with mode numbers between $-n_{\text{max}}$ and n_{max} . As a result, the regularized commutator has the structure

$$[[\hat{V}_1, \hat{H}_0], \hat{V}_1]_{\text{cut}} \propto a n_{\text{max}}^{2\beta^2} \mathbb{I} + n_{\text{max}}^{-2\beta^2} \hat{V}_2 + O(n_{\text{max}}^{-2\beta^2-1}) \quad (21)$$

where \hat{V}_2 corresponds to a perturbation with double frequency:

$$\hat{V}_2 = \int_0^{2\pi} \frac{d\theta}{2} \left(V^{2\beta}(e^{i\theta}, e^{-i\theta}) + V^{-2\beta}(e^{i\theta}, e^{-i\theta}) \right) \quad (22)$$

The contribution of the identity operator is diverging in the limit when the cutoff is eliminated ($n_{\text{cut}} \rightarrow \infty$) and should be renormalized. This can be easily done by considering energy differences only, and then the large ω behaviour can be different depending on how we scale c_1 . We expect the following behaviours:

- If c_1 is not scaled with ω , $c_1 = \lambda$, then the drive averages out and we should see no effect in the spectrum.
- If c_1 is scaled with ω , $c_1 = \lambda\omega$, then we have an effective large ω behaviour, which in energy differences appears as the spectrum of the two-frequency sine-Gordon model. By eliminating the regulator $n_{\text{cut}} \rightarrow \infty$, the extra $\cos 2\beta\phi$ term in the effective potential scales to zero and we again should get back the spectrum of the sine-Gordon theory.
- If, however, we also scale the bare coupling c_1 with the regulator as $c_1 = \lambda\omega E_{\text{cut}}^{\beta^2}$, in order to compensate the factor $n_{\text{max}}^{-2\beta^2}$, then we have a nontrivial large ω and $E_{\text{cut}} \rightarrow \infty$ limit. In this limit, the volume dependence of the new term in the effective potential is

$$\left(\frac{L}{2\pi} \right)^{1-4\beta^2} \frac{\lambda^2}{4} \left(\frac{E_{\text{cut}} L}{2\pi} \right)^{2\beta^2} [[\hat{V}_1, \hat{H}_0], \hat{V}_1] \quad (23)$$

where the dimensionless cut $\hat{E}_{\text{cut}} = \frac{E_{\text{cut}} L}{2\pi}$ is the analogue of n_{max} in this scheme and $\hat{E}_{\text{cut}}^{2\beta^2} [[\hat{V}_1, \hat{H}_0], \hat{V}_1]$ has a finite limit corresponding to the double-frequency cosine operator. The effective theory should then be the two-frequency sine-Gordon model [8]:

$$H_{\text{eff}} = \frac{2\pi}{L} \left[\hat{H}_0 + c_0 \left(\frac{L}{2\pi} \right)^{2-\beta^2} \hat{V}_1 + \left(\frac{L}{2\pi} \right)^{2-4\beta^2} c_2 \hat{V}_2 \right] \quad (24)$$

where $c_2 \propto \lambda^2$ is a scheme-dependent renormalized coupling.

In order to check these behaviours, we develop a novel numerical method. The idea is to combine TCSA with the numerical approach we used in the quantum mechanical case. We thus expand in Fourier components the periodic Floquet wave function in time $u_{\mathcal{E}}(t) = \sum_m u_{\mathcal{E},m} e^{im\omega t}$

and solve the Floquet eigenvalue problem (14) but keeping in mind that now the operators H_0 , V_0 and V_1 act on the conformal Hilbert space. We use the TCSA method to represent these operators with finite matrices on the truncated Hilbert space. Since both the winding number and the momentum is preserved by the perturbation, we focus on the $m = 0$ and $P = 0$ sector. The relevant matrix element of the perturbation are described in Appendix B. In the following section we summarize our findings. All physical quantities are made dimensionless by the soliton mass M .

4 Numerical investigations and results

In this section, we solve numerically both the time-dependent theory at high but finite frequency, and its corresponding time-independent effective theory to support our claims. For a detailed description of the used methods, see Appendix (B).

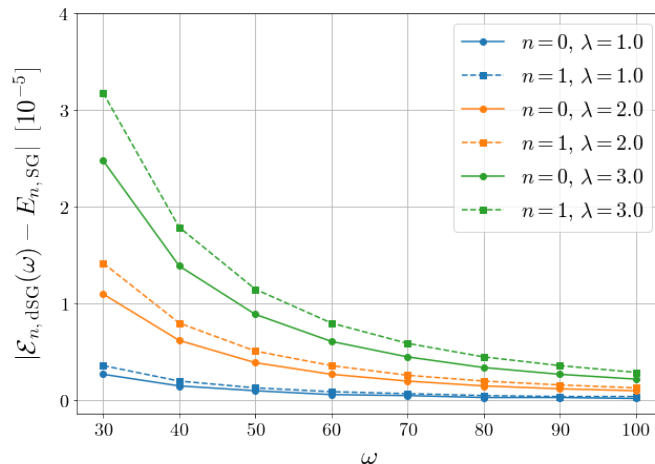


Figure 7: The difference between the quasienergies of the driven and the energies of the original sine-Gordon model for the vacuum and for the first excited state for various $c_1 = \lambda$ values as the function of ω at volume $ML = 14$.

4.1 Floquet quasienergy spectrum

Our first goal is to confirm that the high-frequency expansion is also valid in the continuum limit. In the case when $c_1 = \lambda$, the expansion tells us that the full perturbation vanishes in the high-frequency limit, therefore, from the quasienergies, we should obtain the spectrum of the integrable sine-Gordon theory. This is exactly what we see in Figure 7. Here, we show that for the vacuum ($n = 0$) and the first standing particle ($n = 1$), the difference of the energies tends to zero as the frequency increases independently of the strength of the perturbation.

Let us now turn to the $c_1 = \lambda\omega$ case, where we expect a non-trivial behaviour due to the effect of the $\frac{\lambda^2}{4}[[V_1, H_0], V_1]$ operator. Looking at the full spectrum on Figure 8, we can see that it resembles a meaningful quantum field theory. Knowing that we are in the $m = 0$, $P = 0$ sector, we can identify the vacuum, the standing particles, and the scattering states.

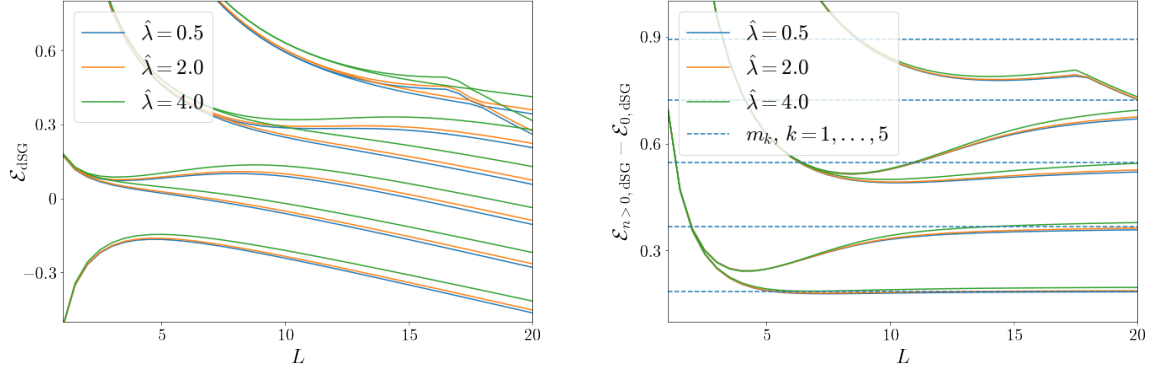


Figure 8: Quasienergy spectrum of the driven sine-Gordon theory for various λ drives ($\omega = 100$). The raw spectrum is on the left, while the groundstate energy subtracted is on the right.

However, comparing it to the sine-Gordon theory, it turns out that the expected non-trivial contribution is just a constant added to every energy level, which does not enrich the dynamics. This also implies that if we subtract the vacuum from every level, we obtain the unperturbed sine-Gordon theory again, and therefore, we have found a strong indication that the infinite-frequency effective correction is a non-vanishing identity in this cutoff scheme too, and the contribution of the \hat{V}_2 operator is negligible.

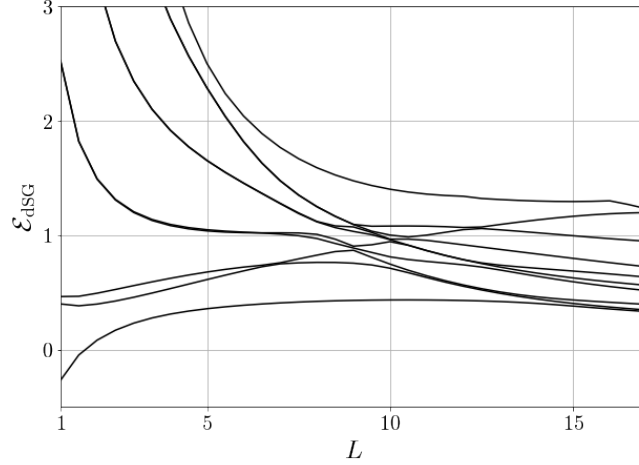


Figure 9: Quasienergy levels of the driven sine-Gordon theory with scaled coupling $c_1 = \lambda\omega E_{\text{cut}}^{\beta^2}$ as the function of the volume. Parameters: $\hat{\lambda} = 14$, $\omega = 100$, $\hat{E}_{\text{cut}} = 19$

In the oscillator mode cutoff scheme, the $c_1 = \lambda\omega E_{\text{cut}}^{\beta^2}$ scaling turned out to be a success in compensating the vanishing \hat{V}_2 operator, however, this is not trivially achieved in the more physical energy cutoff scheme. Thus, we now investigate the effect of such scaling in the time-dependent theory. In Figure 9, we can see that in this case, a metastable state, a so-called false vacuum appears, which is an effect known specifically from the two-frequency

sine-Gordon model [8]. The false vacuum is a vacuum-like energy eigenstate (with linear volume dependence) that has a higher bulk energy, and in this case, we can interpret it as the analogue of the stabilized upper fix point of the Kapitza pendulum. This state can exist in a finite volume., and for larger and larger volumes, it approaches a particle line over the real vacuum. Since this theory is not integrable, the lines avoid each other and the metastable vacuum decays.

Unfortunately, in the parameter region where the time-dependent theory shows the stabilization effect the simulations become more resource demanding and we could not achieve good enough precisions. In order to overcome this, we compare the time-dependent Floquet spectrum to that of the effective time-independent theory.

In Figure 10, we can see the same behaviour as we have seen in the quantum mechanical case (Figure 5): solving the time-dependent Floquet problem and the time-independent effective theory yields the same energies towards the high-frequency limit. We thus in the next subsection focus on a precision analysis of the spectrum of the effective Hamiltonian.

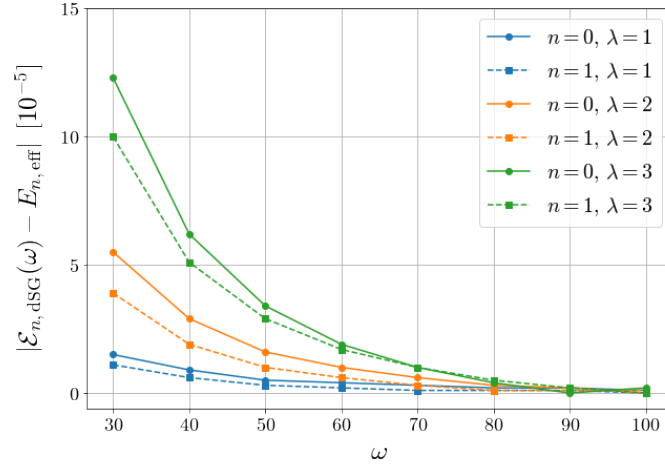


Figure 10: The difference between the quasienergies of the driven and energies of the effective Hamiltonian (20) for the vacuum and the first excited state for various $c_1 = \lambda\omega$ values as the function of ω at dimensionless volume $ML = 14$.

4.2 Effective Hamiltonian

In this section, we analyze the cases when the drive is scaled with the frequency $c_1 = \lambda\omega$ and ω goes to ∞ . The effective Hamiltonian in this limit takes the form

$$\frac{H_{\text{eff}}}{M} = \frac{2\pi}{ML} \left[\hat{H}_0 + \frac{\kappa(\beta^2/2)}{2} \left(\frac{ML}{2\pi} \right)^{2-\beta^2} \hat{V}_1 + \left(\frac{ML}{2\pi} \right)^{2-2\beta^2} \frac{\hat{\lambda}^2}{4} [[\hat{V}_1, \hat{H}_0], \hat{V}_1] \right] \quad (25)$$

where we made the expression dimensionless by dividing by the soliton mass and $\hat{\lambda}$ is the corresponding dimensionless coupling. The TCSA method truncates the Hilbert space at a given energy cut E_{cut} and represents all operators on this truncated Hilbert space by finite

dimensional matrices. As a consequence, the commutator $[[\hat{V}_1, \hat{H}_0], \hat{V}_1]$ is finite, thus regularized, but its matrix elements depend on the energy cutoff. We note that this regularization is not the same which we used in Appendix (B), where we truncated the Hilbert space in the oscillator types (mode numbers) and not in the energy. In that case, arbitrarily large energy states could contribute with small mode numbers.

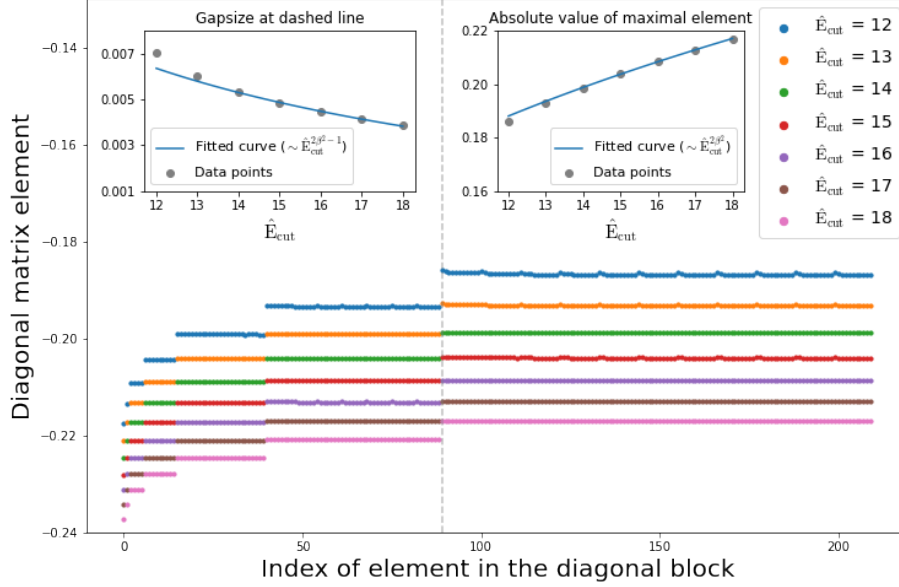


Figure 11: Diagonal elements of the commutator at different energy cuts, when projected back to the Hilbert space at cut = 6. We see that at a given L_0 eigenspace, we basically have an identity operator, however, the relative cutoff dependences of the different L_0 eigenspaces are slightly different and are shifted wrt. each other. The gap between different identity coefficients scales to zero for larger and larger cuts as shown on the left inset. On the right inset we can see how the coefficient of the identity scales with the cut.

In order to understand the cutoff dependence of the commutator, we analyze its matrix elements. Technically, we choose a cutoff and construct the corresponding Hilbert space together with the matrix elements of $[[\hat{V}_1, \hat{H}_0], \hat{V}_1]$. In the next step, we increase the cutoff as well as the representations of \hat{H}_0 and \hat{V}_1 but focus only on the same matrix elements of $[[\hat{V}_1, \hat{H}_0], \hat{V}_1]$. We compare the resulting matrix elements to that of the operators \mathbb{I} and \hat{V}_2 . The Hilbert space has a tensor product form composed of the zero mode and the other oscillators. The commutator in the zero mode space has elements in the diagonal and the second super/subdiagonal blocks, but none of them depends on the value of the zero mode. This enables us to investigate the commutator on a Hilbert space with keeping only the $n = -1, 0, 1$ sectors. We then analyze the cutoff dependence in the other oscillators. In our convention, the cut is an integer which determines the maximal L_0 eigenvalue. We first focus on the diagonal block where we expect the appearance of the identity operator, later we focus on the second subdiagonal block.

Our results for the diagonal part are presented on Figure 4.2. It seems that the diagonal

elements organize themselves into several distinct identity components, corresponding to the L_0 eigenvalues. By increasing the cutoff, the contribution from higher levels decreases and the gap between these components tends to zero. At the same time, the cumulated contributions, namely the absolute value of the maximal element, start to increase. This confirms that in this scheme too, the effective correction contains an identity operator that diverges as the cut increases. By using the data in the cut range 14 – 18, we can fit a curve for the coefficient of the identity component in the form $\sim \hat{E}_{\text{cut}}^{2\beta^2}$ with a high precision. We similarly find that in this range, the gap behaves as $\sim \hat{E}_{\text{cut}}^{2\beta^2-1}$. This confirms that for large cuts the scaling is similar to that of the mode number cutoff scheme.

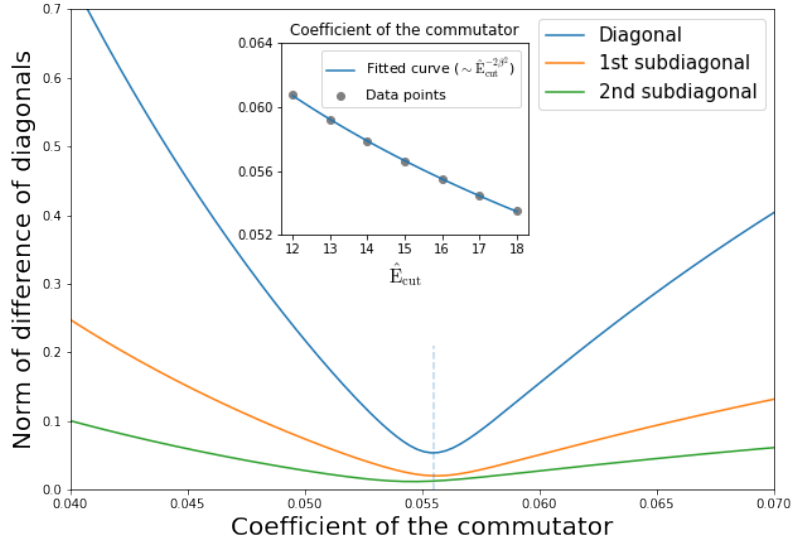


Figure 12: Comparison of the second subdiagonal block of the commutator with the analogues term of the double-frequency cosine matrix. We plot the norm of the diagonal of $x : \cos(2\beta\phi) : - [[\hat{V}_1, \hat{H}_0], \hat{V}_1]$ as the function of x . The minimum in x is basically the same for the first and second subdiagonals. The inset demonstrates the scaling of the minimum as the function of the cut.

By focusing on the second subdiagonal block, we expect the appearance of the matrix elements of the double-frequency cosine operator. In order to confirm this and read off its coefficient, we focus on the diagonal and the first two subdiagonal elements of the block as the entries of the cosine matrix decrease strongly from the diagonal. We take the difference between the diagonals of the commutator and a multiple of the diagonals of the cosine and calculate the norm of the difference, which we plot as a function of the multiple factor. In Figure (4.2), we can see that there is a specific coefficient where the diagonals of the matrices coincide with high precision, which extends also for the first and second subdiagonals. With the so measured proportionality factor, the remaining subdiagonals of the commutator all agree at very high precision with the double-frequency cosine operator. We also measured that this factor decreases with the cut, meaning that the two-frequency contribution becomes

less and less dominant. Again, we could fit a curve of the form $\sim \hat{E}_{\text{cut}}^{-2\beta^2}$ with a very high precision. We therefore conclude that in the energy cutoff scheme, we find the same operators in the effective Hamiltonian as in the oscillator cutoff scheme, and their coefficient also behaves similarly with the increase of the cut.

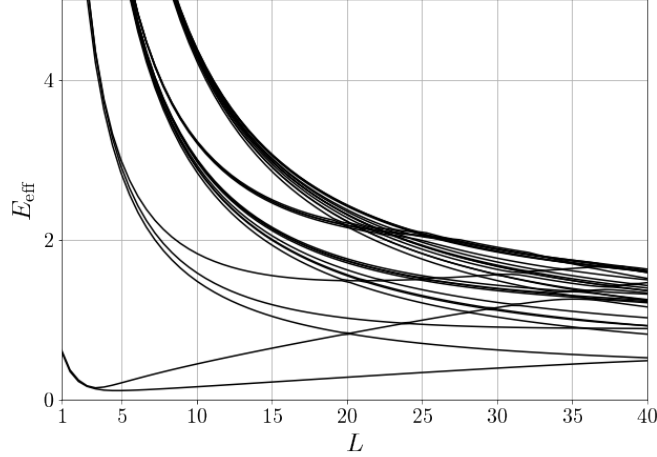


Figure 13: Spectrum of the effective Hamiltonian with the false vacuum which confirms that indeed, the upper unstable equilibrium point turned into an alternate vacuum, just as it happens in the two-frequency sine-Gordon model. Over this vacuum we can recognize a state with the same slope, which can be interpreted as a breather-like excitation over the false vacuum.

All these analyzes convinced us that in the case when we scale $\hat{\lambda}$ as $E_{\text{cut}}^{\beta^2}$ and consider energy differences only, we recover the spectrum of the two-frequency model. Indeed using the operator H_{eff} with the commutator obtained from the highest cut available, we obtained the spectrum on Figure 4.2. This shows without any doubts the presence of the stabilized upper equilibrium point as a false vacuum. We can also recognize an excited state line parallel with this vacuum, which can be interpreted as a standing breather-like excitation over the false vacuum. This is the quantum analogue of the classical solution, which we demonstrated previously.

5 Periodically driven perturbed CFTs

We now extend our analysis from the sine-Gordon model to more general theories. We still investigate theories with Hamiltonians of the form of

$$H = H_0 + V_0 + \cos \omega t V_1 \quad (26)$$

but the unperturbed part is assumed to be a generic conformal field theory

$$H_0 = \frac{2\pi}{L} \hat{H}_0 \quad ; \quad \hat{H}_0 = L_0 + \bar{L}_0 - \frac{c}{12} \quad (27)$$

while the perturbation consists of the integral of relevant spinless ($h_i = \bar{h}_i$) fields, Φ_0 and Φ_1 :

$$V_i = c_i \left(\frac{L}{2\pi} \right)^{1-2h_i} \hat{V}_i \quad ; \quad \hat{V}_j = \int_0^{2\pi} \Phi_j(e^{i\theta}, e^{-i\theta}) d\theta \quad (28)$$

The effective Hamiltonian in the $\omega \rightarrow \infty$ limit takes the generic form (25), which in dimensionless quantities reads as

$$H_{\text{eff}} = \frac{2\pi}{L} \left[\hat{H}_1 + \left(\frac{L}{2\pi} \right)^{2-4h_1} \frac{c_1^2}{4} [[\hat{V}_1, \hat{H}_1], \hat{V}_1] \right] \quad (29)$$

with \hat{H}_1 being the Hamiltonian of the perturbed CFT without the drive

$$\hat{H}_1 = \hat{H}_0 + c_0 \left(\frac{L}{2\pi} \right)^{2-2h_0} \hat{V}_0 \quad (30)$$

The details of calculating the commutator is relegated to Appendix (C). In the simplest case, when $\Phi_0 = \Phi_1$, the identity operator always appears in the operator product expansion (OPE) with a diverging term, which can be renormalized by considering energy differences only, just as we did in the sine-Gordon case. Assuming that the OPE starts as

$$\Phi_1(z, \bar{z})\Phi_1(0, 0) = \frac{1}{(z\bar{z})^{2h_1}} + c_{11}^2 \frac{\Phi_2(0, 0)}{(z\bar{z})^{2h_1-h_2}} + \dots \quad (31)$$

we can scale the amplitude of the drive as $c_1 \propto \lambda \omega E_{\text{cut}}^{h_2-2h_1}$, in order to compensate the dimensions of $(z\bar{z})^{h_2-2h_1}$. The effective large frequency Hamiltonian then takes the form

$$H_{\text{eff}} = \frac{2\pi}{L} \left[\hat{H}_0 + c_0 \left(\frac{L}{2\pi} \right)^{2-2h_0} \hat{V}_0 + c_2 \left(\frac{L}{2\pi} \right)^{2-2h_2} \hat{V}_2 \right] \quad (32)$$

where $c_2 \propto \lambda^2$ is a scheme-dependent effective coupling. This is the Hamiltonian of a conformal field theory perturbed by two operators. Thus the periodic drive in the infinite frequency limit leads to an extra perturbation with an operator, which appears in the OPE of the driven perturbing operator with itself. These theories could be systematically analyzed with the methods of [18]. Our result can lead to very interesting phenomena and would open a new field for the Floquet engineering. In particular, in the critical Ising theory, it would imply that harmonically changing the magnetic field would induce an effective temperature perturbation.

6 Conclusion

In this paper, we investigated the periodically driven sine-Gordon quantum field theory, which is considered to be the continuum limit of coupled many Kapitza pendula. We focused on the large frequency behaviour and determined the Floquet quasienergy spectrum for various driving protocols. By exploiting the perturbed CFT nature of the sine-Gordon model, we combined the TCSA method with the usual numerical Floquet analysis in order to get a tool to determine the quasienergy spectrum of the driven sine-Gordon theory for various driving frequencies. In the large frequency limit, we compared the results with an analytical calculation

based on the large frequency expansion of the effective Hamiltonian. As we found complete agreement, we analyzed the spectrum of this effective Hamiltonian, which is non-trivial and ω -independent if we scale the drive with ω . With this driving protocol, we observed a uniform cutoff-dependent shift in the energy spectrum compared to the original sine-Gordon theory. In order to have a non-trivial effect of the drive in energy differences, we had to scale the drive also with an appropriate power of the energy cutoff. With this protocol, the drive had a marked effect on the spectrum, which stabilized when we increased the cutoff. The resulting quasienergy spectrum agreed with the spectrum of the two-frequency sine-Gordon theory. In particular, we observed the signature of another vacuum in the spectrum with higher bulk energy constant. This other state exists for any volumes, but does not have an infinite volume limit. It corresponds to the upper equilibrium point of the coupled pendula, which got dynamically stabilized by the periodic drive. We even observed an excitation over this false vacuum.

Our investigations and methods can be easily generalized to other periodically driven conformal field theories. Indeed, we already made the first step into this direction. We calculated the effective Hamiltonian in the case when the drive is proportional to ω and an appropriate power of the energy cutoff. In the case when a conformal field theory is perturbed with a spinless relevant operator, Φ_1 via a harmonic time-dependent coupling, the resulting theory is time independent and has two relevant spinless perturbations, Φ_1 and Φ_2 . The second perturbation Φ_2 corresponds to the first non-trivial operator appearing in the product of Φ_1 with itself. In particular, it implies that by perturbing the critical Ising model with a harmonic magnetic field, the effective theory contains an additional thermal perturbation. It would be very interesting to explore the consequences of our findings in real systems. Also, assuming that we harmonically drive a conformal field theory, we can have an effective theory with a single perturbation, which actually can be integrable. One example is the driven sine-Gordon theory with $c_0 = 0$.

In the present paper, we were satisfied by establishing that the appropriately scaled, harmonically driven sine-Gordon theory is equivalent to the two-frequency sine-Gordon model. This correspondence, however, can be explored further. Since the two-frequency model has a plenty of interesting phenomena including phase transitions and new states in the spectrum [7, 8, 19], we expect similar behaviour from the driven model, too. As the driven sine-Gordon theory can be realized in cold atom experiments, it would be very interesting to investigate the experimental consequences of the appearing two-frequency sine-Gordon model.

Acknowledgements

We thank Zoltán Rácz for suggesting the problem and the useful discussions and the NKFIH grant K134946 for support. The work was supported also by ELKH, while the infrastructure was provided by the Hungarian Academy of Sciences.

A Large frequency expansion and a numerical approach

Floquet theorem ensures that the solution of the time-dependent Schrödinger equation

$$i\frac{\partial\Psi}{\partial t} = H\Psi \quad ; \quad H = H_0 + V_0 + \cos\omega t V_1 \quad (33)$$

has the form

$$\psi_{\mathcal{E}}(\phi, t) = e^{-i\mathcal{E}t} u_{\mathcal{E}}(\phi, t) \quad ; \quad u_{\mathcal{E}}(\phi, t + T) = u_{\mathcal{E}}(\phi, t) \quad (34)$$

where the quasienergy \mathcal{E} governs the slow motion in an effective potential, while the periodic $u_{\mathcal{E}}$ is the analogue of the fast modulation. In order to find the effective Hamiltonian, one can make a periodic gauge transformation [9] of the form

$$u_{\mathcal{E}}(\phi, t) = e^{-iF(t)} v_{\mathcal{E}}(\phi) \quad ; \quad H_{\text{eff}} = e^{iF} H e^{-iF} - i(\partial_t e^{iF}) e^{-iF} \quad (35)$$

where F and H_{eff} can be calculated simultaneously order by order in ω^{-1} :

$$F = \omega^{-1} F_1 + \omega^{-2} F_2 + \dots \quad ; \quad H_{\text{eff}} = H_{\text{eff}}^{(0)} + \omega^{-1} H_{\text{eff}}^{(1)} + \omega^{-2} H_{\text{eff}}^{(2)} + \dots \quad (36)$$

by using that

$$e^{iF} H e^{-iF} = H + i[F, H] - \frac{1}{2}[F, [F, H]] + \dots \quad ; \quad (\partial_t e^{iF}) e^{-iF} = i\partial F - \frac{1}{2}[F, \partial F] + \dots \quad (37)$$

and demanding that H_{eff} is time-independent. At the leading order, the time dependent part of H can be cancelled by F_1 as

$$H_{\text{eff}}^{(0)} = H_0 + V_0 \quad ; \quad F_1 = \sin \omega t V_1 \quad (38)$$

At the subleading order, one can ensure $H_{\text{eff}}^{(1)} = 0$ by choosing $F_2 = -i \cos \omega t [V_1, H_0 + V_0]$. At the next order, F_3 can compensate terms only with vanishing average leading to an effective term

$$H_{\text{eff}}^{(2)} = \frac{1}{4} [[V_1, H_0 + V_0], V_1] \quad (39)$$

In order to test the large frequency approximation in the case of the Kapitza pendulum, we determine numerically the Floquet basis, which satisfies the modified Schrödinger equation:

$$H_F u_{\mathcal{E}}(\phi, t) = \mathcal{E} u_{\mathcal{E}}(\phi, t) \quad ; \quad H_F = H - i\partial_t \quad (40)$$

Since $u_{\mathcal{E}}(\phi, t)$ is periodic in time, we simply expand it in Fourier components:

$$u_{\mathcal{E}}(\phi, t) = \sum_m u_{\mathcal{E},m}(\phi) e^{im\omega t} \quad (41)$$

such that the eigenvalue problem takes the form

$$(m\omega + H_0 + V_0) u_{\mathcal{E},m} + \frac{1}{2} V_1 (u_{\mathcal{E},m-1} + u_{\mathcal{E},m+1}) = \mathcal{E} u_{\mathcal{E},m} \quad (42)$$

We can further expand $u_{\mathcal{E},m}(\phi)$ in the eigenbasis of H_0 : $u_{\mathcal{E},m}(\phi) = \sum_n c_{m,n} |n\rangle$ which are nothing but the momentum eigenstates $p_{\phi} |n\rangle = n |n\rangle$, which take the form $|n\rangle = \frac{1}{\sqrt{2\pi}} e^{in\phi}$. Since the matrix elements of V_0 and V_1 are explicitly calculable $e^{\pm i\phi} |n\rangle = |n \pm 1\rangle$, the eigenvalue problem reduces to

$$(m\omega + \frac{n^2}{2}) c_{m,n} + \frac{c_0}{2} (c_{m,n-1} + c_{m,n+1}) + \frac{c_1}{4} (c_{m-1,n-1} + c_{m+1,n-1} + c_{m-1,n+1} + c_{m+1,n+1}) = \mathcal{E} c_{m,n} \quad (43)$$

Technically, we truncate the tensor product Hilbert space both in m and n to take values between $|m| < m_{\text{max}}$ and $|n| < n_{\text{max}}$ and diagonalize numerically the finite Hamiltonian. The quasienergy is defined only modulo ω as we can change $\mathcal{E} \rightarrow \mathcal{E} \pm \omega$ by shifting m . This implies that we find any eigenvalue and eigenvector many times. We thus restrict the eigenspectrum by demanding $0 \leq \mathcal{E} < \omega$, what we call the fundamental region, and order the states wrt. the time average of the expectation value of the energy $\langle H \rangle$ over one driving period.

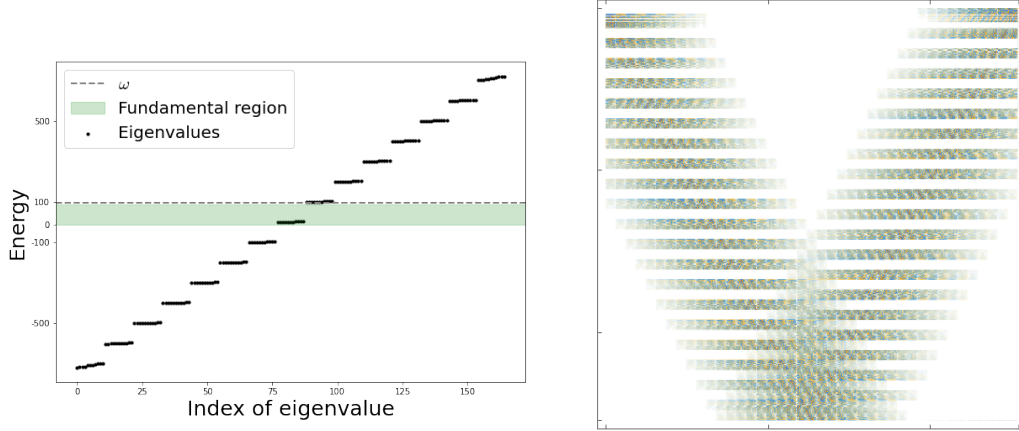


Figure 14: On the left, there is a plot of the eigenvalues of the Kapitza pendulum obtained from our method. The same eigenvalues appear with shifts of integer multiples of ω , but we only use the central, so-called fundamental region, which contains all the states with maximal precision. On the right, there is a plot of the elements of the matrix that diagonalizes the finite Hamiltonian. Its rows correspond to eigenvectors, and one can see that practically, different blocks contain the same numbers, but they belong to different Fourier modes. These shifts eventually cancel out when one sums up the time-dependent solution, and they result in the same physical states.

B TCSA and the driven sine-Gordon model

The quantum version of the periodically driven sine Gordon model is defined by its Hamiltonian (14) with (15). Since ϕ is an angle variable boundary conditions can be labeled by the integer winding number m as $\phi(x + L, t) = \phi(x, t) + 2\pi r m$, which distinguishes topological sectors. Within each sector we expand the field as

$$\phi(x, t) = 2\pi m r \frac{x}{L} + \sum_{n=-\infty}^{\infty} \phi_n(t) e^{in \frac{2\pi}{L} x} \quad (44)$$

The zero mode ϕ_0 behaves as a single pendulum. In the free theory its conjugate momentum π_0 , satisfying $[\pi_0, \phi_0] = -i$, has the spectrum $\pi_0|n\rangle = \frac{n}{r}|n\rangle$ with periodic wave functions $e^{i \frac{n}{r} \phi_0}$ in ϕ_0 . The other modes ϕ_n can be expanded in terms of creation and annihilation operators. Since the free massless boson is a conformal field theory the field separates into independent left and right moving parts:

$$\phi(z, \bar{z}) = \varphi(z) + \bar{\varphi}(\bar{z}) \quad ; \quad \varphi(z) = \frac{\phi_0}{2} - i\pi_0 \log z + i \sum_{n \neq 0} a_n \frac{z^{-n}}{n} \quad (45)$$

and similarly with $z \leftrightarrow \bar{z}$ and $a \leftrightarrow \bar{a}$ for $\bar{\varphi}$. Canonical commutation relations imply that

$$[a_n, a_m] = n\delta_{n+m} \quad ; \quad [\bar{a}_n, \bar{a}_m] = n\delta_{n+m} \quad ; \quad [a_n, \bar{a}_m] = 0 \quad (46)$$

and the Hilbert space is built over the states with given winding and momentum numbers by acting with the left and right moving creation operators (16). The normal ordered Hamiltonian

and momentum can be written in terms of the oscillators as in (17). The perturbing operator, having mapped to the plane, takes the form (18), where the normal ordered vertex operator

$$V^\beta(z, \bar{z}) =: e^{i\beta\phi(z, \bar{z})} := V_0^\beta V_-^\beta V_+^\beta \quad (47)$$

can be factorized into the zero mode

$$V_0^\beta(z, \bar{z}) = e^{i\beta\phi_0}(z\bar{z})^{\beta\pi_0} \quad (48)$$

and the creation-annihilation parts

$$V_\mp^\beta(z, \bar{z}) = \prod_{n>0} e^{\pm\beta a_{\mp n} \frac{z^{\pm n}}{n}} \prod_{n>0} e^{\pm\beta \bar{a}_{\mp n} \frac{\bar{z}^{\pm n}}{n}} \quad (49)$$

In calculating the effective Hamiltonian (20) we need to evaluate $[[\hat{V}_1, \hat{H}_0], \hat{V}_1]$, where the dimension-less conformal Hamiltonian is $H_0 = \frac{2\pi}{L} \hat{H}_0$ and the dimensionless part of V_1 is

$$\hat{V}_1 = \int_0^{2\pi} \frac{d\theta}{2} \left(V^\beta(e^{i\theta}, e^{-i\theta}) + V^{-\beta}(e^{i\theta}, e^{-i\theta}) \right) \quad (50)$$

We start to calculate $[\hat{H}_0, V^\beta(z, \bar{z})]$, with $V^\beta(z, \bar{z}) = V_0^\beta V_-^\beta V_+^\beta$. Using the commutation relations we obtain

$$\begin{aligned} [\hat{H}_0, V^\beta(z, \bar{z})] &= [\pi_0^2, V_0^\beta] V_-^\beta V_+^\beta + \sum_{n>0} (V_0^\beta [a_{-n} a_n, V_-^\beta] V_+^\beta + V_0^\beta V_-^\beta [a_{-n} a_n, V_+^\beta]) \\ &= \beta(J_-(z, \bar{z}) V^\beta(z, \bar{z}) + V^\beta(z, \bar{z}) J_+(z, \bar{z})) \\ &= \beta^2 V^\beta(z, \bar{z}) + (z\partial + \bar{z}\bar{\partial}) V^\beta(z, \bar{z}) \end{aligned} \quad (51)$$

where we introduced

$$J_\mp(z, \bar{z}) = \pi_0 + \sum_{n>0} (a_{\mp n} z^{\pm n} + \bar{a}_{\mp n} \bar{z}^{\pm n}) \quad (52)$$

In calculating the next commutator we obtain

$$[J_\mp(z, \bar{z}), V^\beta(w, \bar{w})] = \beta \left(1 + \sum_{n>0} z^{\pm n} w^{\mp n} + \sum_{n>0} \bar{z}^{\pm n} \bar{w}^{\mp n} \right) V^\beta(w, \bar{w}) \quad (53)$$

In particular, when we calculate the effective Hamiltonian we need terms of the form

$$\begin{aligned} [[\hat{H}_0, V^\alpha(z, \bar{z})], V^\beta(w, \bar{w})] &= \alpha[J_-(z, \bar{z}) V^\alpha(z, \bar{z}) + V^\alpha(z, \bar{z}) J_+(z, \bar{z}), V^\beta(w, \bar{w})] \\ &= \text{terms multiplying } [V^\alpha(z, \bar{z}), V^\beta(w, \bar{w})] \\ &\quad + \alpha\beta \left(\sum_n z^n w^{-n} + \sum_n \bar{z}^n \bar{w}^{-n} \right) V^\alpha(z, \bar{z}) V^\beta(w, \bar{w}) \end{aligned} \quad (54)$$

Let us note that $V^\alpha(z, \bar{z}) =: e^{i\alpha\phi(z, \bar{z})} : \propto e^{i\alpha\phi(z, \bar{z})}$ where the proportionality is a regulator dependent c-number. Since the equal time commutator of ϕ with itself is vanishing

$$[\phi(x, t), \phi(x', t)] = 0 \quad (55)$$

the commutator of two vertex operator does not contribute. Furthermore we know the operator product expansion of the vertex operator

$$V^\alpha(z, \bar{z})V^\beta(w, \bar{w}) = (z - w)^{\alpha\beta}(\bar{z} - \bar{w})^{\alpha\beta} (V_{\alpha+\beta}(w, \bar{w}) + (z - w)\partial V_{\alpha+\beta}(w, \bar{w}) + \dots) \quad (56)$$

where we indicated the first descendant. Recalling that we have to integrate eventually with $z = e^{i\theta}$, $\bar{z} = e^{-i\theta}$ and $w = e^{i\theta'}$ and $\bar{w} = e^{-i\theta'}$ on the unit circle:

$$\int_0^{2\pi} \int_0^{2\pi} d\theta d\theta' \sum_n e^{in(\theta-\theta')} (2 - e^{i(\theta-\theta')} - e^{-i(\theta-\theta')})^{\alpha\beta} V_{\alpha+\beta}(e^{i\theta'}, e^{-i\theta'}) + \dots \quad (57)$$

If we would sum up in n from $-\infty$ to ∞ , then we could use that $\sum_n e^{in\theta} = 2\pi\delta(\theta)$. This actually implies that the integral is 0 if $\alpha\beta > 0$ or it is ∞ if $\alpha\beta < 0$. In our case $\alpha = \pm\beta$ and we always face a divergent behaviour. In order to regularize this we introduce a cutoff in n and analyze the dependence on this cut. The θ integral is periodic and we can evaluate as

$$\int_0^{2\pi} d\theta e^{in\theta} (2 - 2\cos\theta)^{\alpha\beta} = \frac{\pi \sec(\pi\alpha\beta)\Gamma(n - \alpha\beta)}{\Gamma(-2\alpha\beta)\Gamma(\alpha\beta + n + 1)} \quad (58)$$

It is symmetric in n and the large n behaviour is

$$\frac{\Gamma(n - \alpha\beta)}{\Gamma(\alpha\beta + n + 1)} = n^{-1-2\alpha\beta} \left(1 - \frac{1 + 2\alpha\beta}{n} + \dots \right) \quad (59)$$

This implies that the sum behaves as

$$\sum_{n=-n_{\max}}^{n_{\max}} \frac{\Gamma(n - \alpha\beta)}{\Gamma(\alpha\beta + n + 1)} \propto n_{\max}^{-2\alpha\beta} \quad (60)$$

We need to analyze two cases. For $\alpha = \beta$ the sum is convergent and goes to zero. For the leading term in the OPE it goes to zero quite slowly as $\beta^2 < 1$, however, for descendant the exponent is shifted by an integer, thus it goes to zero much faster. For $\alpha = -\beta$ the sum is divergent. For the leading term in the OPE, which contains the identity, it diverges again slowly as $\beta^2 < 1$. For descendants it is again convergent.

Let us point out that the introduction of the cutoff n_{\max} physically means that we keep only oscillators, which create particles with conformal energies smaller than n_{\max} . We allow however an arbitrary number of these particles showing that the cut is not an energy cut. In this regularization scheme the effective Hamiltonian has the structure

$$H_{\text{eff}}^{(2)} \propto \frac{1}{4} [[\hat{V}_1, \hat{H}_0], \hat{V}_1] \propto an_{\max}^{2\beta^2} \mathbb{I} + n_{\max}^{-2\beta^2} \hat{V}_2 + O(n_{\max}^{-2\beta^2-1}) \quad (61)$$

where \hat{V}_2 corresponds to a perturbation with double frequency:

$$\hat{V}_2 = \int_0^{2\pi} d\theta \frac{1}{2} \left(V^{2\beta}(e^{i\theta}, e^{-i\theta}) + V^{-2\beta}(e^{i\theta}, e^{-i\theta}) \right) \quad (62)$$

Finally, let us develop a numerical method to check these behaviours. The idea is the same as in the quantum mechanical case. We Fourier expand the periodic Floquet wave function in time $u_{\mathcal{E}}(t) = \sum_m u_{\mathcal{E},m} e^{im\omega t}$ and solve the Floquet eigenvalue problem (14) but now the

operators H_0, V_0 and V_1 act on the conformal Hilbert space. We use the TCSA method to represent these operators with finite matrices on the truncated Hilbert space. The relevant matrix element of the perturbation are as follows. The zero mode has matrix elements

$$\langle n, m | V_0^{\pm\beta} | n', m' \rangle = \delta_{m, m'} \delta_{n, n' \pm 1} \quad (63)$$

while for the s^{th} oscillator we have

$$\langle n, m | a_s^l e^{\pm\beta a_{-s}/s} e^{\mp\beta a_s/s} a_{-s}^k | n, m \rangle = \sum_{i=\max(0, k-l)}^k \binom{k}{i} (-1)^i s^{k-i} (k-i)! (\pm\beta)^{l-k+2i} \binom{l}{k-i} \quad (64)$$

These states should be normalized with the square root of $\langle 0 | a_s^l a_{-s}^k | 0 \rangle = \delta_{l,k} k! s^k$. The truncated Hilbert space is defined to keep states below a given energy cutoff. Thus this is not equivalent to keep oscillators below a given n_{\max} as even a single oscillator has states with arbitrarily large energies.

Although we were only interested in the infinite frequency limit, where it is enough to diagonalize the much smaller matrices of the effective theory, our method is applicable to general frequencies, where the dynamics can be much more complex. In this case, the time-dependence increases the size of the matrices such that implementing an algorithm that can handle them can easily become a challenging task.

In our implementation, we used the PRIMME [20, 21] C-package that was specifically designed for large-scale eigenvalue problems. PRIMME has an interface that only needs a function that realizes a matrix-vector multiplication, thus giving the user the complete freedom of representing the matrix. This allows us to exploit the double tensor product structure of the Hilbert space so that we only have to store a single block of elements of V_0 , which reduces the memory costs to a level that is also sufficient for a general purpose computer.

C Calculation of the effective Hamiltonian for generic perturbed CFTs

In this appendix we calculate the effective Hamiltonian for generic perturbation of CFTs (29). In doing so we recall that

$$[L_0, \Phi(z, \bar{z})] = h\Phi(z, \bar{z}) + z\partial_z\Phi(z, \bar{z}) \quad (65)$$

and similar relations for \bar{L}_0 with \bar{z} , which are considered to be independent, but put to $z = e^{i\theta}$ and $\bar{z} = e^{-i\theta}$ at the end of the calculation. The standard trick in calculating the equal time commutator [22] is to exploit the fact that products of operators are well-defined only when they are radially ordered, the analogue of time ordering after the exponential mapping. Thus the commutator can be replaced by radially ordered products, i.e. by deforming the z_1 integration around the unit circle C_1 : a bit increasing the radius in the first and decreasing in the second term as:

$$\oint_{C_1} dz_1 \oint_{C_1} dz_2 [\Phi_1(z_1, \bar{z}_2), \Phi_2(z_2, \bar{z}_2)] = \left(\oint_{C_{1+\epsilon}} \oint_{C_1} - \oint_{C_{1-\epsilon}} \oint_{C_1} \right) dz_1 dz_2 R(\Phi_1(z_1, \bar{z}_1), \Phi_2(z_2, \bar{z}_2)) \quad (66)$$

As usual, we do not indicate radial ordering explicitly any more. Radially ordered products have the operator product expansion (OPE)

$$\Phi_1(z_1, \bar{z}_1)\Phi_2(z_2, \bar{z}_2) = c_{12}^i \frac{1}{((z_1 - z_2)(\bar{z}_1 - \bar{z}_2))^{h_1+h_2-h_i}} \Phi_i(z_2, \bar{z}_2) + \dots \quad (67)$$

Since z and \bar{z} are considered to be independent, not the complex conjugate of each other, when we take $|z_1| > 1$ we have to also take $|\bar{z}_1| > 1$. This implies that the contributions from $z_1 = (1 + \epsilon)e^{i\theta_1}$, $\bar{z}_1 = (1 + \epsilon)e^{-i\theta_1}$ and from $z_1 = (1 - \epsilon)e^{i\theta_1}$, $\bar{z}_1 = (1 - \epsilon)e^{-i\theta_1}$ cancel each other. This is not true when we perform the same calculations with $z_1\partial_{z_1}\Phi_1$ (or with $\bar{z}_1\partial_{\bar{z}_1}\Phi_1$) instead of Φ_1 as these derivatives introduce an unbalanced pole of the form of $1/(z_1 - z_2)$ or $1/(\bar{z}_1 - \bar{z}_2)$. The difference of the integration contours results in a delta function $2\pi i\delta(z_1 - z_2)$. This is the analogue of the $\delta(\theta_1 - \theta_2) = \sum_n e^{in(\theta_1 - \theta_2)}$ term in (57). When calculated without an energy cutoff, the delta function puts θ_1 to θ_2 leading to zero/infinite depending on the sign of $h_1 + h_2 - h_i$ in complete analogy with the similar results in the sine-Gordon theory. In order to get a finite and non-trivial result, we have to scale the amplitude of the drive c_1 appropriately with the cutoff.

Depending on the rich spectrum of the CFT we can expect numerous interesting cases. In the following, however, we focus only on the simplest, namely when $\Phi_0 = \Phi_1$. In this case the identity operator always appears in the OPE with a diverging term, which can be renormalized by considering energy differences only, just as we did in the sine-Gordon case. Assuming that the OPE starts as

$$\Phi_1(z, \bar{z})\Phi_1(0, 0) = \frac{1}{(z\bar{z})^{2h_1}} + c_{11}^2 \frac{\Phi_2(0, 0)}{(z\bar{z})^{2h_1-h_2}} + \dots \quad (68)$$

we can scale the amplitude of the drive as $c_1 \propto \lambda\omega E_{\text{cut}}^{h_2-2h_1}$, in order to compensate the dimensions of $(z\bar{z})^{h_2-2h_1}$. The effective large frequency Hamiltonian then takes the form

$$H_{\text{eff}} = \frac{2\pi}{L} \left[\hat{H}_0 + c_0 \left(\frac{L}{2\pi} \right)^{2-2h_0} \hat{V}_0 + c_2 \left(\frac{L}{2\pi} \right)^{2-2h_2} \hat{V}_2 \right] \quad (69)$$

where $c_2 \propto \lambda^2$ is a scheme-dependent effective coupling.

References

- [1] G. Mussardo, Statistical Field Theory, Oxford Graduate Texts, Oxford University Press, 2020.
- [2] A. Mitra, Quantum quench dynamics, Annual Review of Condensed Matter Physics 9 (1) (2018) 245–259. doi:10.1146/annurev-conmatphys-031016-025451.
- [3] M. Bukov, L. D’Alessio, A. Polkovnikov, Universal high-frequency behavior of periodically driven systems: from dynamical stabilization to floquet engineering, Advances in Physics 64 (2) (2015) 139–226. doi:10.1080/00018732.2015.1055918. URL <http://dx.doi.org/10.1080/00018732.2015.1055918>
- [4] K. P. L., Dynamic stability of a pendulum when its point of suspension vibrates, Soviet Phys. JETP. 21 (1951) 588–597.

- [5] R. Citro, E. G. Dalla Torre, L. D'Alessio, A. Polkovnikov, M. Babadi, T. Oka, E. Demler, Dynamical stability of a many-body kapitza pendulum, *Annals of Physics* 360 (2015) 694–710. doi:10.1016/j.aop.2015.03.027.
URL <http://dx.doi.org/10.1016/j.aop.2015.03.027>
- [6] V. P. Yurov, A. B. Zamolodchikov, Truncated conformal space approach to scaling Lee-Yang model, *Int. J. Mod. Phys. A* 5 (1990) 3221–3246. doi:10.1142/S0217751X9000218X.
- [7] G. Delfino, G. Mussardo, Nonintegrable aspects of the multifrequency Sine-Gordon model, *Nucl. Phys. B* 516 (1998) 675–703. arXiv:hep-th/9709028, doi:10.1016/S0550-3213(98)00063-7.
- [8] Z. Bajnok, L. Palla, G. Takacs, F. Wagner, Nonperturbative study of the two frequency sine-Gordon model, *Nucl. Phys. B* 601 (2001) 503–538. arXiv:hep-th/0008066, doi:10.1016/S0550-3213(01)00067-0.
- [9] S. Rahav, I. Gilary, S. Fishman, Effective hamiltonians for periodically driven systems, *Phys. Rev. A* 68 (2003) 013820. doi:10.1103/PhysRevA.68.013820.
URL <https://link.aps.org/doi/10.1103/PhysRevA.68.013820>
- [10] G. Feverati, F. Ravanini, G. Takacs, Truncated conformal space at $c = 1$, nonlinear integral equation and quantization rules for multi - soliton states, *Phys. Lett. B* 430 (1998) 264–273. arXiv:hep-th/9803104, doi:10.1016/S0370-2693(98)00543-7.
- [11] L. Samaj, Z. Bajnok, Introduction to the statistical physics of integrable many-body systems, Cambridge University Press, Cambridge, 2013.
- [12] G. Fodor, P. Forgacs, Z. Horvath, A. Lukacs, Small amplitude quasi-breathers and oscillons, *Phys. Rev. D* 78 (2008) 025003. arXiv:0802.3525, doi:10.1103/PhysRevD.78.025003.
- [13] A. B. Zamolodchikov, Mass scale in the sine-Gordon model and its reductions, *Int. J. Mod. Phys. A* 10 (1995) 1125–1150. doi:10.1142/S0217751X9500053X.
- [14] C. Destri, H. J. de Vega, Nonlinear integral equation and excited states scaling functions in the sine-Gordon model, *Nucl. Phys. B* 504 (1997) 621–664. arXiv:hep-th/9701107, doi:10.1016/S0550-3213(97)00468-9.
- [15] G. Feverati, F. Ravanini, G. Takacs, Nonlinear integral equation and finite volume spectrum of Sine-Gordon theory, *Nucl. Phys. B* 540 (1999) 543–586. arXiv:hep-th/9805117, doi:10.1016/S0550-3213(98)00747-0.
- [16] A. B. Zamolodchikov, Two point correlation function in scaling Lee-Yang model, *Nucl. Phys. B* 348 (1991) 619–641. doi:10.1016/0550-3213(91)90207-E.
- [17] G. Delfino, P. Simonetti, J. L. Cardy, Asymptotic factorization of form-factors in two-dimensional quantum field theory, *Phys. Lett. B* 387 (1996) 327–333. arXiv:hep-th/9607046, doi:10.1016/0370-2693(96)01035-0.

- [18] G. Delfino, G. Mussardo, P. Simonetti, Nonintegrable quantum field theories as perturbations of certain integrable models, Nucl. Phys. B 473 (1996) 469–508. [arXiv:hep-th/9603011](#), [doi:10.1016/0550-3213\(96\)00265-9](#).
- [19] G. Takacs, F. Wagner, Double sine-Gordon model revisited, Nucl. Phys. B 741 (2006) 353–367. [arXiv:hep-th/0512265](#), [doi:10.1016/j.nuclphysb.2006.02.004](#).
- [20] A. Stathopoulos, J. R. McCombs, PRIMME: PReconditioned Iterative MultiMethod Eigensolver: Methods and software description, ACM Transactions on Mathematical Software 37 (2) (2010) 21:1–21:30.
- [21] L. Wu, E. Romero, A. Stathopoulos, Primme_svds: A high-performance preconditioned SVD solver for accurate large-scale computations, SIAM Journal on Scientific Computing 39 (5) (2017) S248–S271.
- [22] P. H. Ginsparg, Applied Conformal Field Theory, in: Les Houches Summer School in Theoretical Physics: Fields, Strings, Critical Phenomena, 1988. [arXiv:hep-th/9108028](#).